Complexes of Adenosine Deaminase with Two Potent Inhibitors: X-ray Structures in Four Independent Molecules at pH of Maximum Activity[†,‡]

Zhongmin Wang and Florante A. Quiocho*

Structural and Computational Biology and Molecular Biophysics Program, Howard Hughes Medical Institute, and Verna and Marrs McLean Department of Biochemistry, Baylor College of Medicine, Houston, Texas 77030

Received February 9, 1998; Revised Manuscript Received April 10, 1998

ABSTRACT: Adenosine deaminase, which catalyzes the irreversible hydrolytic deamination of adenosine nucleosides to inosine nucleosides and ammonia, is a key enzyme in purine metabolism and lymphoid development. The X-ray structures of murine adenosine deaminase with bound potent inhibitors (K_i values $\approx 10^{-13}$ M) (8*R*)-hydroxyl-2′-deoxycoformycin (pentostatin), a transition state analogue, and (6*S*)-hydroxyl-1,6-dihydropurine riboside, a reaction coordinate analogue, have been determined and refined to resolutions of 2.6 and 1.95 Å, respectively. Crystals of both complexes were obtained at pH 7, where the enzyme is fully active, in an identical space group with the asymmetric unit containing four molecules. In addition to the very high degree of similarity between the four independent molecules in each complex structure, there is also considerable structural similarity of the complex with the dihydropurine riboside with that of an identical complex previously determined at pH 4.2 where the enzyme is 20% active. The interactions between the enzyme and the two analogues are extremely similar. These include the coordination of the *8R*- or *6S*-hydroxyl group of the analogues to the Zn^{2+} which mainly contributes to the strong potency and very high degree of stereospecificity of inhibition by these analogues. The interactions are further indicative of the structural and chemical requirements of substrates. These structures and recent site-directed mutagenesis have further shed light on the catalytic mechanism of the enzyme.

Adenosine deaminase (ADA)[1] has attracted considerable attention since its existence, and some aspects of its specificity were first reported about 65 years ago (1). ADA is a monomeric protein (40 kDa) which catalyzes the irreversible hydrolytic deamination of adenosine nucleosides to their respective inosine nucleosides and ammonia. Catalysis requires a Zn^{2+} cofactor (2).

About 30 years ago, coformycin (8*R*-hydroxyl isomer) isolated in the culture filtrates of *Norcardia interforma* and *Streptomyces kaniharaensis*, was demonstrated as a potent inhibitor ($K_i \approx 10^{-10}$ M) of ADA (*3*). Ten years after this discovery, pentostatin or (8*R*)-hydroxyl-2′-deoxycoformycin (DCF) (Figure 1), isolated from the fermentation broth of *Streptomyces antibioticus* (*4*), was shown to be a 1−2 order of magnitude stronger inhibitor than coformycin (*5*, *6*). The strong inhibitory effect of these two natural products provided one aspect of the early evidence for the idea that they represent analogues of the transition state. As both coformycin and DCF possess a tetrahedral carbon (C8) at the position corresponding to C6 of adenosine (Figure 1), they represent transition-state analogues. The potency of DCF is greatly dependent on the stereochemistry at the hydroxyl-bearing C8 position; the 8*R* isomer binds about 10^7 times stronger than the 8*S* isomer (*7*). DCF is often used clinically to increase the effectiveness of various antitumor and antiviral analogues of adenosine. It has also been used to treat patients with hairy cell leukemia (*8*, *9*). One of the two structures reported here for the first time is that of ADA with bound DCF.

ADA is present in virtually all mammalian tissues. Lack of ADA activity is associated to severe combined immunodeficiency disease (SCID), a genetically inherited disease fatal to newly born children if not properly diagnosed and treated (*10*). Higher levels of ADA in the alimentary tract and decidual cells of the developing fetal-maternal interface put ADA among those enzymes performing unique roles related to the growth rate of cells, embryo implantation, and other undetermined functions (*11*−*13*).

With a k_{cat} of 375 s^{-1} and a k_{cat}/K_m of 1.4×10^7 M^{-1} s^{-1} (*14*), the reaction that ADA catalyzes is close to being encounter limited. It is believed that the reaction proceeds by hydroxide addition to C6 of adenosine to form a tetrahedral intermediate and elimination of ammonia to generate the inosine product (*15*−*17*).

The X-ray structure of ADA is the first for a purine/pyrimidine deaminase enzyme (*2*). ADA has a $(\beta/\alpha)_8$ barrel structural motif. As seen in over 30 unrelated enzymes with this motif, the active site of ADA resides at the C-terminal end of the β barrel, in a deep oblong-shaped pocket. A pentacoordinated Zn^{2+} cofactor is embedded in the deepest part of the pocket. The unexpected discovery of a bound

[†] Supported by Howard Hughes Medical Institute and a grant from NSF (STI-9512521).

[‡] Coordinates have been deposited in the Brookhaven Protein Data Bank (code 1a4m and 1a41)

* To whom correspondence should be addressed. HHMI-Baylor, Houston, TX 77030. Fax: 713-798-8516. E-mail: faq@dino.bcm.tmc.edu.

[1] Abbreviations: ADA, adenosine deaminase; DAA, 1-deazaadenosine; CDA, cytidine deaminase; DCF, (8*R*)-hydroxyl-2′-deoxycoformycin; HDPR, (6*S*)-hydroxyl-1,6-dihydropurine ribonucleoside; PR, purine ribonucleoside.

S0006-2960(98)00324-9 CCC: $15.00
Published on Web 05/19/1998

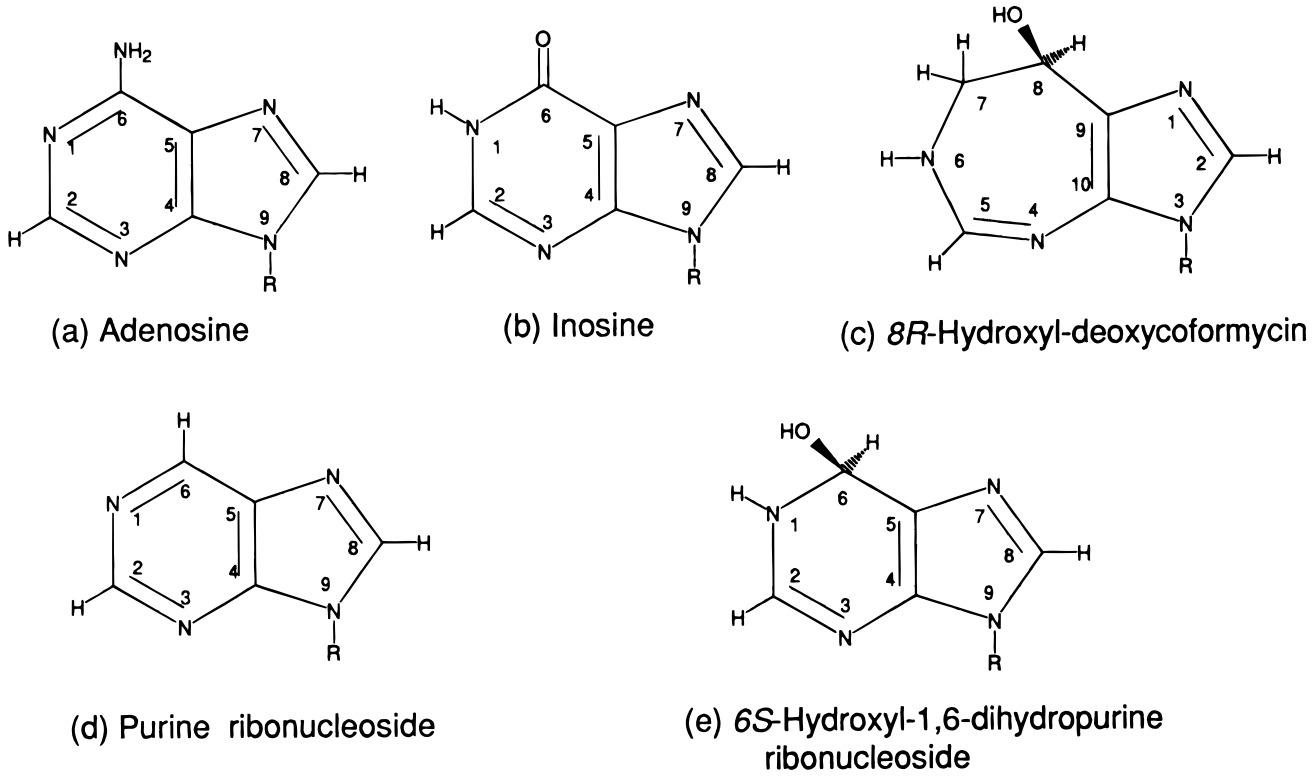

FIGURE 1: Schematic diagrams: (a) adenosine, (b) inosine, (c) (8*R*)-hydroxyl- deoxycoformycin, (d) purine ribonucleoside or riboside, and (e) (6*S*)-hydroxyl-1,6-dihydropurine ribonucleoside. The sugar substituent, R, in DCF is 2′-deoxy-ribose, whereas those of the other compounds are ribose.

Zn^{2+} prompted the demonstration of stoichiometric amount of the cation in other purine/pyrimidine deaminases (*18*−*20*).

Although ADA was crystallized and harvested in the presence of the inhibitor purine riboside (PR) (Figure 1), the ligand bound in the active site is 6-hydroxyl-1,6-dihydropurine ribonucleoside (HDPR) (Figure 1). HDPR is derived by an enzyme-catalyzed stereospecific addition of a Zn^{2+}-activated water molecule or hydroxide to the C6 position of PR (*2*). A Zn^{2+}-bound hydroxide has in fact been observed in the structure of ADA complexed with 1-deazaadenosine (DAA) (*21*), a ground-state analogue (*14*, *22*). Seven residues are within hydrogen-bonding distance to the HDPR, of which three (Glu 217, Asp 295, and His 238), combined with the Zn^{2+}, are directly implicated in catalysis.

HDPR is considered to be a nearly ideal transition-state analogue with an estimated K_i of about 10^{-13} M (*23*, *24*). Binding comparisons between HDPR and 1,6-dihydronebularine showed that the 6-hydroxyl group of HDPR contributes −9.8 kcal/mol to the free energy of binding. It is the chelation of the 6-hydroxyl group to the Zn^{2+} that contributes to the very high estimated affinity of HDPR (*2*) rather than the formation of a hydrogen bond to a carboxylate side chain as proposed by Kati and Wolfenden (*24*).

All previous X-ray structures of native and mutant ADA were determined from crystals obtained at pH 4.2 (*2*, *21*, *25*), where the enzyme in solution is only about 20% active (*26*). Nevertheless, the observation that the enzyme converts PR to HDPR at this pH demonstrates catalytic competency, especially in the first reaction phase of stereospecific hydroxide addition. While it is most desirable to crystallize proteins under conditions of maximum activity, such as pH, absence of high concentration of salts, which are often used as a precipitant, and a crystal lattice with no crystal force influencing the ligand binding or active site, this is very often difficult to achieve given little or no control and the unpredictability of the crystallization processes. Here, we report the structures of the complexes of ADA with DCF and HDPR from crystals obtained at pH 7 where the enzyme is fully active (*26*, *27*). Moreover, as structures of both complexes were determined in a crystal form with four independent molecules in the asymmetric unit, the crystal lattice effect is not a factor, and the redundancy provides a good measure of the accuracy of the structure. The catalytic mechanism of ADA is discussed in light of these structures.

MATERIALS AND METHODS

Protein Preparation and Crystallization. Recombinant murine ADA was purified as described previously (*28*). DCF was generously provided by Parke Davis Co., and PR was purchased from Sigma Chemical.

Both ADA crystals in the presence of DCF or PR were grown at pH 7 and 4 °C using the hanging drop vapor diffusion technique. All solutions were adjusted to pH 7.0 before and after mixing. The solutions placed in the wells were measured approximately every other day during the entire period of crystal growth to ensure that the pH remains at neutrality.

In the crystallization of ADA in the presence of PR, the 6 μL drops contained 8.2 mg/mL protein, 20 mM PR, 6.7% PEG 3350, 33 mM NaCl, and 33 mM HEPES buffer at pH 7.0. The 0.5 mL solution in the well was composed of 20% PEG 3350, 100 mM NaCl, and 100 mM HEPES at pH 7.0. After 4−5 days of equilibration, each drop was seeded with

Table 1: Diffraction Data and Structure Refinement Statistics of ADA with Bound Ligands

	HDPR	DCF
diffraction data		
resolution (Å)	1.95	2.6
reflections measured/unique	415 190/83 321	330 776/47 806
R-sym (no sigma cutoff)		
overall/outer shell	0.078/0.401	0.095/0.249
completeness (%)		
overall/outer shell	70.2/47	96/94
refinement statistics		
data with $\|F\| > 2\sigma(\|F\|)$		
resolution range/reflections	10.0−1.95/77 948	8.0−2.6/43 502
R-factor	0.193	0.185
R-free	0.281	0.272
rms deviations		
bond length (Å)	0.009	0.008
bond angle (deg)	1.474	1.516
dihedrals (deg)	23.087	23.067
avg *B*-factor (Å^2), for four molecules, excluding water molecules	16.96	13.38

a microcrystal, which grew to a size of about 0.2 × 0.3 × 0.8 mm in 4−5 weeks. A similar procedure was used in crystallizing ADA in the presence of DCF (5 mM).

Prior to data collection, a crystal was successively transferred into a well solution containing increasing amounts of glycerol (5, 10, and 15%) and flash-cooled to −170 °C with a Molecular Structure Corporation cryogenic unit. Diffraction data were collected using a MAC Science DIP2030 two image plate system with a double-mirror focusing optics mounted on a Rigaku RU-200 rotating anode (CuKα) operated at 50 kV and 90 mA.

Both crystals of ADA obtained in the presence of PR and DCF are isomorphous, exhibiting a $P2_1$ space group. The unit cell dimensions in the presence of PR are $a = 88.693$ Å, $b = 93.644$ Å, $c = 102.177$ Å, and $\beta = 102.838°$, and those in DCF complex are $a = 88.929$ Å, $b = 93.355$ Å, $c = 101.953$ Å, and $\beta = 102.941°$. The V_m coefficient of both crystals is 2.6 Å^3/Da with four molecules in one asymmetric unit, indicating about 65% water content. This form of the pH 7 crystals is different from that of the pH 4.2 crystals used previously in structural studies of native ADA with bound ligands (*C*2 space group with one molecule in the asymmetric unit) (*2*, *21*, *25*).

The two diffraction data sets, which were processed using DENZO and SCALEPACK (*29*), gave the statistics shown in Table 1. The diffraction of the crystal in the presence of PR exhibits the highest resolution (1.95 Å) that has been achieved for ADA structures thus far.

Structure Determination and Refinement. The first of the two structures to be determined is that of ADA crystallized in the presence of PR, henceforth identified as its hydrated product, HDPR. It was determined by molecular replacement using XPLOR Version 3.84 (*30*) and the pH 4.2 ADA−HDPR structure (*2*) excluding the bound HDPR ligand and ordered water molecules as the search model. The Zn^{2+} cofactor was included in the search to increase the weight of the model.

Self-rotation functions showed a peak with about half the height of the origin peak. After solving the structure, it became apparent that this peak corresponds to a noncrystallographic symmetry 2-fold element at spherical angles $\psi = 90°$, $\phi = 77.5°$, and $\kappa = 180°$. The cross-rotation search using the intensity data from 15 to 4 Å yielded two top peaks (Eulerian angles are $\theta_1 = 89°$, $\theta_2 = 82°$, $\theta_3 = 87°$ and $\theta_1 = 269°$, $\theta_2 = 78°$, $\theta_3 = 88°$) with rotation function values of 4.34 and 4.26, respectively.

With four molecules in the asymmetric unit, it was suspected that two pairs are related by translation. Translation functions confirmed this suspicion; with the two cross-rotation function solutions, the translation functions yielded two top solutions with 10.8σ and 6.3σ above the mean, respectively. These two solutions had fractional coordinates $x = 0.175$, $y = 0.000$, $z = 0.475$ and $x = 0.650$, $y = 0.439$, $z = 0.425$.

The molecular replacement model was refined using the XPLOR program version 3.85 (*30*), with the model restrained by the Engh and Huber stereochemical parameters (*31*). In the refinement of the ADA−HDPR complex against the highest resolution data (1.95 Å), a random sample containing about 10% of the total data (7814 out of 77 948 unique reflections) was excluded from the refinement. *R*-free, the agreement between calculated and observed structure factors for these reflections, was used to provide an unbiased indicator of the accuracy of the model and to monitor the course of the refinement.

Rigid-body refinement of the molecular replacement model, without the bound HDPR inhibitor, using 30 846 reflections between 10 and 3 Å brought the *R*-factor down to 32% from an initial value of 56%. After extending the data to the highest resolution (1.95 Å), a simulated annealing procedure followed by several rounds of alternating positional and *B*-factor refinements and model adjustments reduced the *R*-factor to around 23%. Water molecules were added with automated water-picking routine in XPLOR and inspected in CHAIN version 7.2 (*32*). The refinement to 1.95 Å resolution converged to an *R*-factor of 19.2% and *R*-free of 29.4%.

All electron density maps calculated with $2|F_o| - |F_c|$ and $|F_o| - |F_c|$ at this stage of the refinement showed the presence of a large well-ordered density in the active site, in all four independent molecules, to which a HDPR molecule with normal bond distances and angles as obtained in the structure at pH 4.2 (*2*) could easily be fitted.

To improve the accuracy and geometry of the model, as assessed by the *R*-free (*33*, *34*), further refinement was undertaken using bulk solvent correction and loose noncrystallographic symmetry restraint. Moreover, excluded from the model used in the first 10 cycles of alternating positional and temperature factor refinements were the HDPR, Zn^{2+}, four residues (His 15, His 17, His 214, and Asp 295) liganding the Zn^{2+}, and two additional residues (Glu 217 and His 238) previously inferred to play roles in catalysis (*2*).

A bulk solvent mask correction in XPLOR (*35*) was justified because of the high solvent content of the structure (about 65%). The validity of this approach was monitored by the change in *R*-factor and *R*-free, especially in the low-resolution shell. The *R*-factor dropped slightly from 18.9 to 18.4% overall and from 14.6 to 12.7% in the resolution range of 3.8 to 10.0 Å. The *R*-free decreased from 29.4 to 28.3% overall and from 26.5 to 22.5% in the resolution range of 3.8 to 10.0 Å.

A loose NCS restraint with an effective energy weight of 300 kcal mol^{-1} Å^{-2} implemented in XPLOR (*36, 37*) not only reduced the *R*-free (from 28.3 to 27.3%), but also gave better geometrical parameters. At the same time, the *R*-factor rose to give a smaller difference between *R*-factor and *R*-free.

The unbiased electron density maps calculated with $2|F_o| - |F_c|$ and $|F_o| - |F_c|$ revealed very well-ordered density for the residues, Zn^{2+}, and HDPR omitted in the model. As the omitted coordinates fit the density very well, they were included in the model and several rounds of XPLOR refinement were carried out. In the final stage of the refinement, the NCS restraint energy was gradually released by a step of 100 kcal mol^{-1} Å^{-2} while the *R*-factor, *R*-free, and the geometry of the structure were closely monitored and electron density maps were examined. The release of NCS restraints resulted in a slight increase of *R*-free and a lower *R*-factor with no significant change in the geometry parameters.

The DCF-bound structure was solved by direct phasing with the ADA−HDPR complex structure with the contribution of the bound ligand and water molecules omitted. Rigid-body refinement brought the *R*-factor from 30 to 25%. Simulated annealing and several rounds of alternating positional and *B*-factor refinement, together with the addition of water molecules, converged to an *R*-factor of 21.2% and an *R*-free of 28.3%. The bulk solvent correction and NCS restraints helped in the fitting, especially to the density of DCF, using the small molecule crystal structure (*38*) as the model, to its density in $2|F_o| - |F_c|$ and $|F_o| - |F_c|$ maps. In the final round of refinement, the NCS restraints were released slowly using a similar procedure to that of HDPR complex. The final statistics of both structures are shown in Table 1.

RESULTS

Structure Determination and Comparison. The structure with the bound HDPR was refined against the 1.95 Å resolution data to an *R*-factor of 19.3% and *R*-free of 28.1%. The DCF-bound structure was similarly refined against the 2.6 Å data to an *R*-factor of 18.5% and an *R*-free of 27.2%. The atomic models, for the four independent molecules (named A, B, C, and D), in both complexes have good stereochemistry. All four molecules in both structures include 349 out of 352 residues, one Zn^{2+} cofactor, and the inhibitor bound in the active site. Only the first three residues have uninterpretable electron density and, hence, are missing in the final models. The main-chain dihedral angles of four nonglycine residues, all with well-defined density, for four independent molecules in both structures, fall outside of the allowed region of the Ramachandran diagram. Interestingly, of these four residues, two (Asp 295 and His 238) are in the active site and likely involved in catalysis (see below). This feature exists in all previous structures of ligand-bound wild-type and mutant ADA from crystals obtained at pH 4.2 and in different space groups (*2, 21, 25, 39, 40*).

Consistent with well-ordered structures, the overall average *B*-factor for all protein atoms, Zn^{2+}, and bound ligand in the asymmetric unit of the ADA−HDPR complex structure is 16.96 Å^2 (Table 1). The average temperature factor of each of the four independent molecules deviates no more than 0.6% of the overall. The average temperature factor of the four molecules in the ADA−DCF complex structure is 13.38 Å^2, with each molecule deviating less than 2%.

There is very high similarity between the four independent ADA molecules in each complex structure. The average rms separations of superimposed equivalent α-carbon atoms and all atoms of the protein, HDPR, and Zn^{2+}, for all four molecules, in the ADA−HDPR structure are 0.23 (0.03) Å and 0.36 (0.04) Å, respectively. Similarly, the average rms deviations in the ADA−DCF structures are 0.25 (0.03) Å for equivalent α-carbon atoms and 0.37 (0.03) Å for all atoms. The deviations in α-carbon atoms and all atoms of the A molecules in both complex structures are 0.21 and 0.43 Å, respectively. The rms difference in α-carbon atoms of the A molecule of the ADA−HDPR structure at pH 7 and the single molecule of the same complex at pH 4.2 (*2*) is 0.27 Å.

Zn^{2+} Coordination. Zn^{2+} is found in more than 50 different proteins/enzymes, of which over 20 have had their 3-D structures determined (*41*). Although Zn^{2+} is found coordinated to six water molecules in solution, it is mainly involved in four or five coordination in the active sites of enzymes, including contributions from bound water molecules and inhibitors.

Until now, the geometry of the Zn^{2+} coordination has not been described in detail. The availability of the 1.95 Å structure of the ADA−HDPR, the highest resolution structure obtained thus far, and the opportunity to compare with the structures of ADA with bound DCF and DAA (*21*) provided the impetus for the detailed description that follows. As shown in Figure 2 and Table 2, the Zn^{2+} is coordinated by three NE2s from imidazole side chains (His 15, His 17, and His 214), one OD2 from a carboxylate (Asp 295), and one hydroxyl from the bound ligand (6-OH in HDPR or 8-OH in DCF) or hydroxide observed in the structure of ADA−DAA complex (*21*). To our knowledge, this is the first time that this coordination motif composed of this group of atoms is observed for a catalytic Zn^{2+}. A similar motif, composed only of the four residues (no water molecule), has been observed for the structural Zn^{2+} bound in superoxide dismutase (*42*).

The Zn^{2+} coordination geometry, with bound HDPR, was initially deduced to be nearly tetrahedral with the three His NE2s occupying three vertexes and the Asp 295 OD2 and the ligand hydroxyl group sharing the fourth site (*2*). However, a detailed examination, with Table 2 and Figure 2, shows that the coordination geometry best fits a trigonal bipyramid with the NE2 atoms of His 15 and His 17, and 6-OH of HDPR, 8-OH of DCF, or OH^- molecule in the bound DAA structure occupying the vertexes of the triangle, and His 214 NE2 and Asp 295 OD2 occupying the apexes. Whereas the locations of the coordinating atoms from the side chains and inhibitors at each of the five positions are very similar, the position of the bound hydroxide is shifted from those of the hydroxyl groups of the inhibitors (Figure 2).

The averages of the distances, for all four independent molecules, from the protein ligands to the Zn^{2+} is 2.46 (0.08) Å in the complex with HDPR and 2.51 (0.15) Å in that with DCF. In contrast, the averages from the inhibitor ligands appear shorter, 2.21 (0.07) Å from the HDPR O6 and 1.90

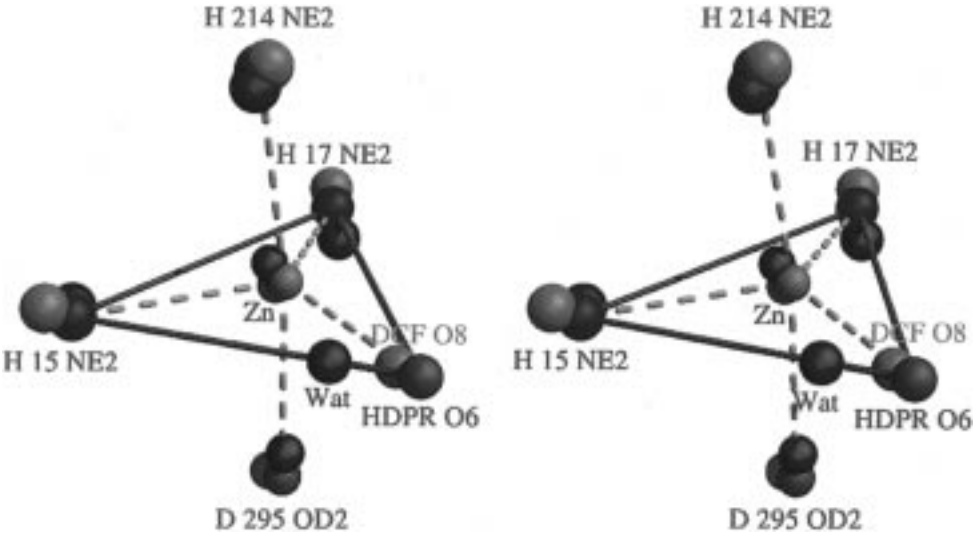

FIGURE 2: Trigonal bipyramid coordination of the Zn^{2+} in the active site of ADA. Stereoview of the coordination in the structures of ADA with bound HDPR (color coded atoms: Zn^{2+}, gold; O, red; N, blue), DCF (all gray atoms) and 1-deazaadenosine with bound H_2O or OH^- (all green atoms) (*21*). This view is based on least-squares superpositioning of atoms shown for the three structures. This figure and those of 3, 4, and 5 were produced using the MidasPlus program (*51*).

Table 2: Zn^{2+} Coordination in the pH 7 Structures of ADA Complexed with HDPR and DCF (Average for Four Independent Molecules)

A. Distances (Å)

residue/ligand	HDPR structure	DCF structure
His 15 NE2	2.48 (0.07)	2.64 (0.11)
His 17 NE2	2.46 (0.23)	2.51 (0.10)
His 214 NE2	2.54 (0.08)	2.60 (0.08)
Asp 295 OD2	2.34 (0.06)	2.30 (0.09)
HDPR O6/DCF O8	2.21 (0.07)	1.90 (0.04)

B. Angles (deg)[a]

Zn^{2+}	His 15 NE2	His 17 NE2	His 214 NE2	Asp 295 OD2	HDPR O6
His 15 NE2		119.6 (7.8)	90.1 (5.6)	84.6 (5.7)	117.1 (0.8)
His 17 NE2	122.8 (5.1)		87.2 (7.3)	100.0 (5.2)	122.1 (7.0)
His 214 NE2	87.5 (3.9)	87.8 (7.3)		171.5 (2.1)	98.8 (5.1)
Asp 295 OD2	85.4 (2.0)	102.2 (5.2)	168.8 (5.4)		79.2 (1.4)
DCF O8	114.0 (2.4)	122.9 (4.7)	94.7 (3.7)	81.1 (3.3)	

[a] Angles in the upper-right half are found in the ADA−HDPR complex and those in the lower-left half are in the ADA−DCF complex.

(0.04) Å from the DCF O8 (Tables 2). These shorter distances likely reflect the extremely tight binding of both inhibitors. The distance from the hydroxide to the Zn^{2+} in the structure of ADA−DAA complex is similarly short (1.91 Å) (*21*).

Interestingly, all of the Zn^{2+} coordinating residues are further involved in other interactions (not shown). Hydrogen bonds are formed between His 15 ND1 and Glu 260 OE1, His 17 ND1 and HDPR or DCF 5′-OH, His 214 ND1 and Asp 181 OD1, and Asp 295 OD1 and Ser 265 OG.

Complexes of ADA with HDPR and DCF at pH 7. In both structures, the ligands have very well-defined electron density for four independent molecules (e.g., Figures 3a and 4a). The four independent active sites in the ADA−HDPR complex are some of the most ordered regions of the models and have almost identical geometry. The site with residues, zinc, HDPR, and two water molecules, as depicted in Figure 3, has an average temperature factor, for four independent models, of 12.2 (0.9) $Å^2$, which is even lower than that of the entire four independent structures (Table 1). The average rms deviation of the atoms in the site, for four molecules, is 0.20 (0.02) Å which is much better than that of all atoms of the proteins, Zn^{2+}, and HDPR. Moreover, as shown in Figure 3, the active site in the structure at pH 7, where the enzyme is fully active, is very similar to that in the initial structure at pH 4.2 (*2*), where the enzyme is 20% active. As the rms deviation of the atoms in the active site of the pH 7 (molecule A) and the pH 4.2 molecule is 0.23 Å, the interactions of the HDPR in the active site are extremely well preserved in the two structures (Table 3). These interactions are also very similar to those in the structure of a crystal of ADA−HDPR complex obtained at pH 4.2 and titrated to pH 6 (Table 3) (*26*).

In light of the above findings, the suggestion by the groups of Wolfenden and Carter that the ADA structure at pH 4.2 represents an inactive form (*44*) is unfounded. Lacking any merit is also the suggestion by these groups that crystal packing forces favor an inactive configuration at pH 4.2. In fact, the active site in the pH 4.2 structure is nowhere near a symmetry-related molecule and is capable of catalyzing the hydration of PR. The pH 7 structures of the complexes with HDPR and DCF remove any reservation about the configuration of the active site. Moreover, all ADA crystals (including those described here) were obtained in the absence of high salt concentration. In contrast, CDA was crystallized in 30% saturated ammonium sulfate (*43*).

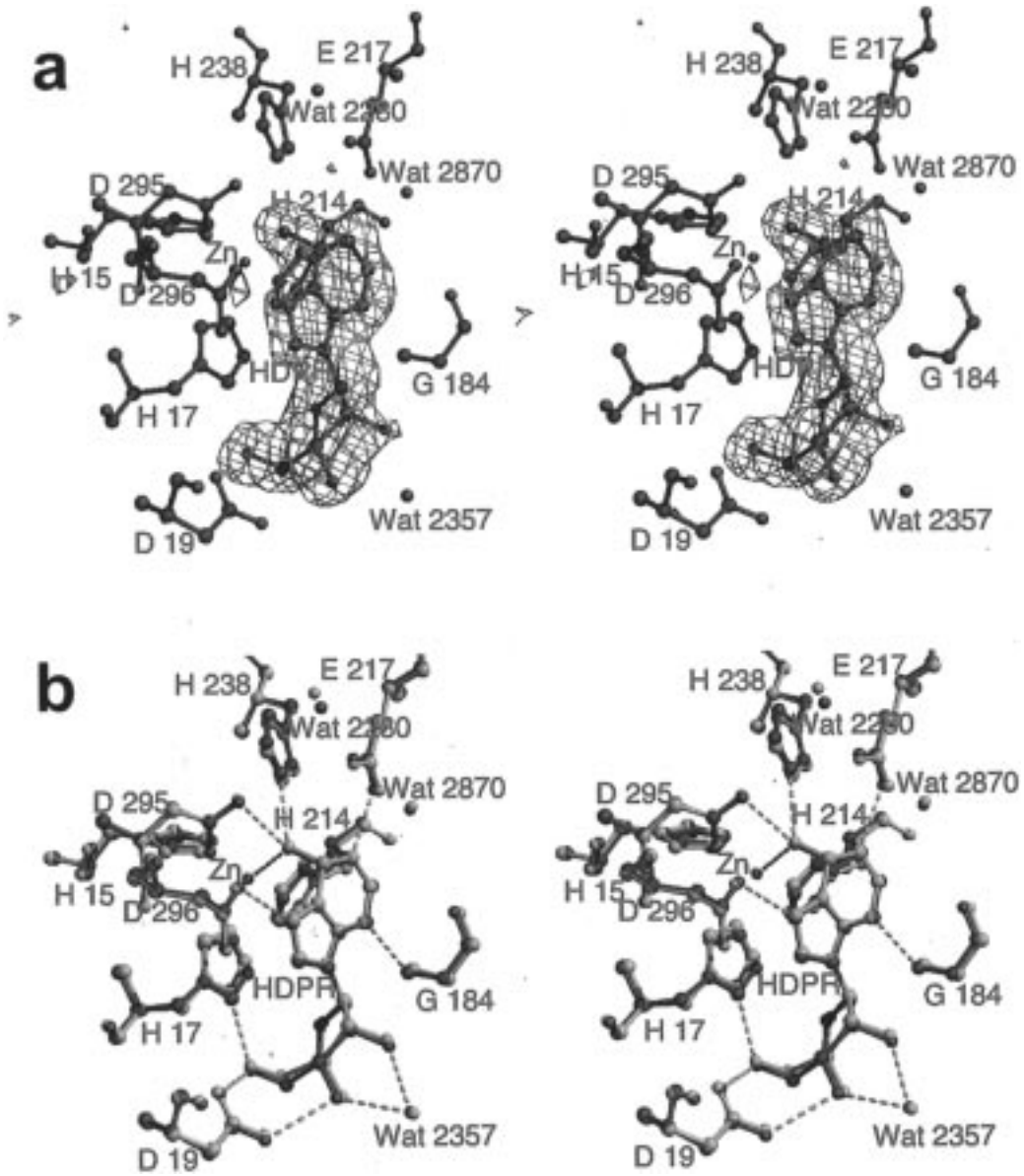

FIGURE 3: Stereo drawing of the binding of HDPR to ADA in the structure at pH 7. (a, top) Difference electron density map (yellow) of the bound HDPR. The density was obtained by omitting the HDPR in the structure factor calculation of the final refined structure. (b, bottom) Coordination and hydrogen bond interactions between the HDPR and ADA in the structure at pH 7 (atom color codes: C, green; O, red; N, blue; Zn^{2+}, gold) superimposed with those in the structure at pH 4.2 (all gray atoms) (*2*).

Similar to the ADA−HDPR complex structure, the active site in the ADA−DCF complex structure, for all four molecules, is more ordered than the entire protein structure and exhibits almost identical geometry. The average temperature factor and rms deviation of the atoms in the site, as shown in Figure 4, for four independent models are 8.9 (0.5) $Å^2$ and 0.22 (0.01) Å, respectively.

Bond Length of the C6−O6 of HDPR and C8−O8 of DCF. On the basis of the 2.3 Å structure of CDA with the bound reaction-coordinate analogue zebularine 3-4 hydrate, it was indicated that the bond distance of the C4−O4 of the analogue (the equivalent of C6−O6 of HDPR) is unusually long (∼1.7 Å) (*44*). This distance, whose significance remains a mystery, was arrived at by restraining the target covalent distance of the C4−O4 to 1.6 Å in the refinement using the TNT package (*45*).

We have evaluated the bond distance of the C6−O6 of HDPR following completion of the refinement of both structures with the bound HDPR or DCF exhibiting no abnormal bond distances or geometry. As the DCF structure is accurately known from the small molecule crystal structure analysis (*38*), it served as a control. Indeed, we see no reason for the distance of the preexisting C8−O8 bond of DCF (the equivalent of the C6−O6 of HDPR, Figure 1) to vary from the 1.427 Å obtained in the small molecule crystal structure.

After applying a distance restraint of 1.6 Å to the target covalent bond C6−O6 of HDPR or C8−O8 of DCF, further alternating cycles of positional and *B*-factor refinement in XPLOR were carried out for each structure. The bond length of the C6−O6 of HDPR, for four molecules, increased to 1.60 (0.01) Å from a normal distance of 1.43 Å in the final refined structure. However, the fact that the bond distance of C8−O8 of the bound DCF also increased to 1.60 (0.01) Å casts serious doubts on the validity of the above results, which also include that of CDA. The proximity of the hydroxyl groups to as strong a scatterer as a Zn^{2+} makes

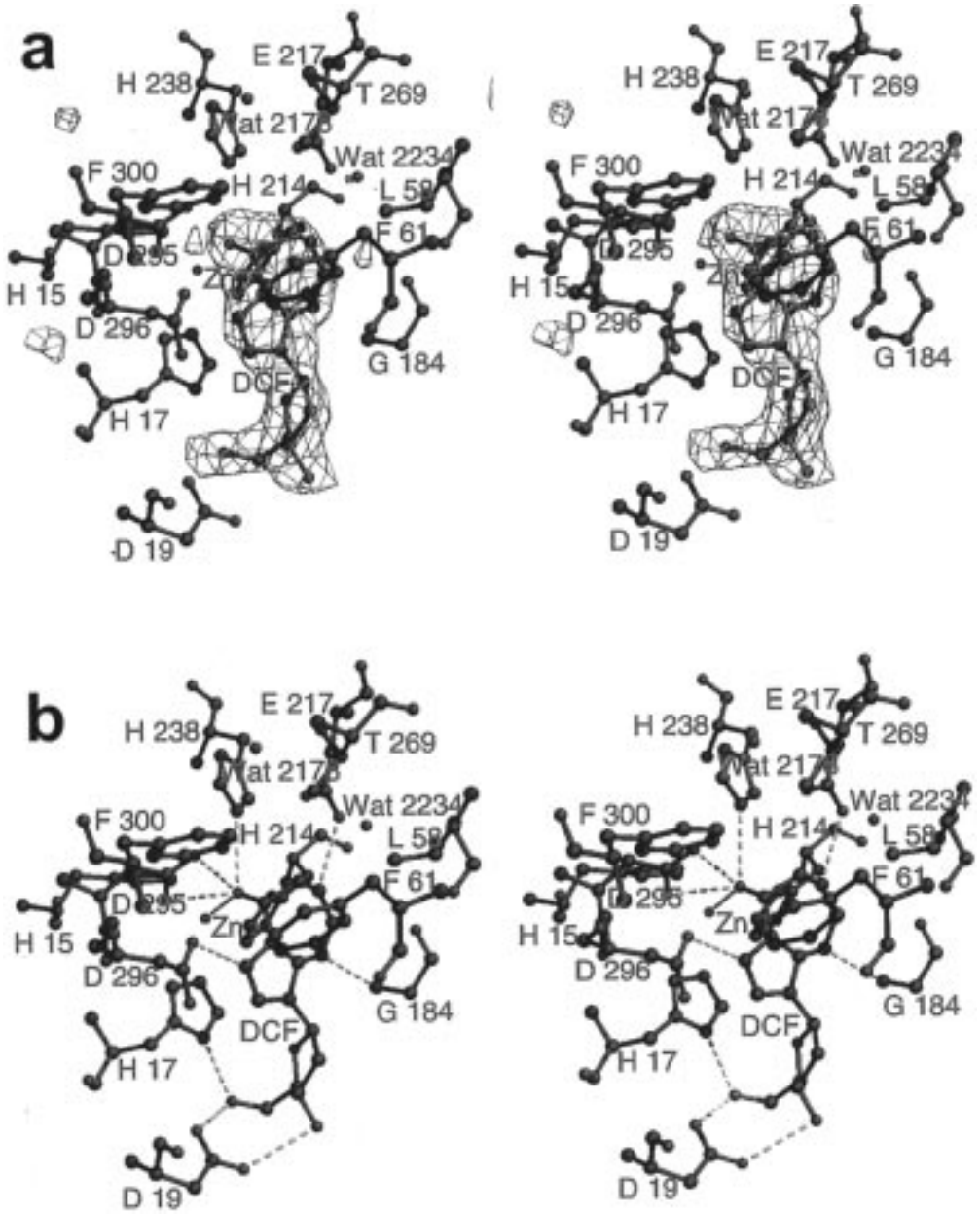

FIGURE 4: Stereo drawing of the interactions between ADA and DCF. (a, top) The difference density (yellow) of DCF superimposed with the refined model. The density was calculated with coefficients ($|F_o| - |F_c|$) and α_c from the final refined structure (Table 1) excluding the contributions of the DCF. (b, bottom) Hydrogen bond and coordination interactions of the polar groups of DCF with ADA and Zn^{2+} (atom color codes: C, green; O, red; N, blue; Zn^{2+}, gold). An 8*S*-hydroxyl group of DCF would be in the vicinity of Leu 58, Phe 61, Thr 269, and Phe 300.

any accurate assessment of the covalent bond distances in question difficult, especially at the relative low resolutions in which the crystallographic analysis of both enzymes were undertaken.

Abundance of Acidic Residues in the Active Site and Strained Conformations. A striking observation is that, of the seven residues engaged in interactions with the HDPR or DCF (Figures 3 and 4), four have acidic side chains (Asp 19, Glu 217, Asp 295, and Asp 296). Interestingly, all these interactions are formed with the side chains in the syn stereochemistry (Figures 3 and 4). This finding is consistent with the observation that syn is the preferred and more favorable orientation in the interactions of these side chains (*46*, *47*). Both of the side-chain oxygens of Glu 217 are further involved in hydrogen-bonding interactions with water molecules, but these interactions are in the anti orientation (Figure 5).

It is noteworthy that Asp 295, as well as His 238, has strained backbone conformation. The ϕ/ψ values of the Asp and His residues in the HDPR-bound structure are 73°/−75° and 80°/−87°, respectively, clearly outside the allowed region. Very similar values are observed in the complex with DCF and in all other structures of ADA, including mutant enzymes, determined thus far.

DISCUSSION

The determination of the structures of complexes of ADA with two potent inhibitors (DCF, a transition-state analogue, and HDPR, a reaction coordinate analog) at a pH of maximum activity has further provided insight to inhibitor binding, substrate recognition, and activity of the enzyme.

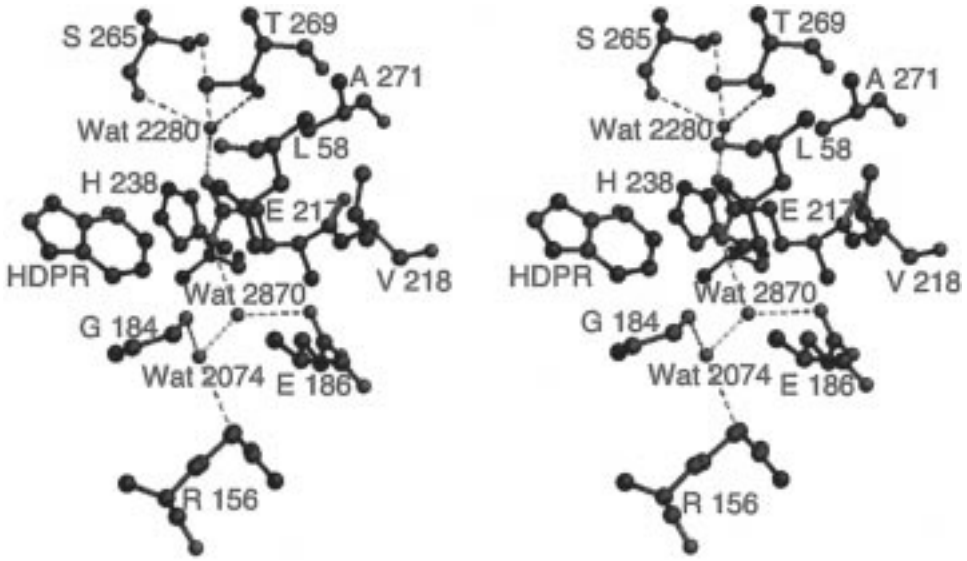

FIGURE 5: Stereoview of the side chain of Glu 217 and its involvement in networks of hydrogen bonds. Also shown are other residues within van der Waals' distance to Glu 217.

Table 3: Distances to the HDPR at the Active Site of ADA

atoms		distances (≤3.3 Å)		
ADA	HDPR	pH 7.0[a]	pH 6.0[b]	pH 4.2[c]
His 17 ND2	O5′	2.51 (0.10)	2.9	2.8
Asp 19 OD1	O5′	2.76 (0.11)	2.6	2.6
Asp 19 OD2	O3′	2.84 (0.08)	3.0	3.0
Gly 184 N	N3	3.05 (0.08)	3.1	3.2
Glu 217 OE1	N1	2.82 (0.05)	2.8	2.8
His 238 NE2	O6	3.25 (0.11)	3.1	3.2
Asp 295 OD1	O6	2.78 (0.04)	2.7	2.7
Asp 296 OD2	N7	2.83 (0.04)	2.7	2.8
Zn^{2+}	O6	2.21 (0.07)	2.1	2.3
H_2O (2357)	O2′	2.85 (0.08)	3.2	3.2
H_2O (2357)	O3′	2.76 (0.10)	2.8	2.9

[a] Average for four independent molecules. [b] The crystal was obtained at pH 4.2 (*2*) and equilibrated to pH 6.0 (*26*). [c] Obtained from ref *2*.

Table 4: Hydrogen Bond and Coordination Distances to DCF at the Active Site of ADA

atoms		
ADA	DCF	distances (Å)[a]
His 17 ND1	O5′	2.54 (0.04)
Asp 19 OD1	O5′	2.86 (0.16)
Asp 19 OD2	O3′	2.99 (0.27)
Gly 184 N	N4	3.26 (0.08)
Glu 217 OE1	N6	2.92 (0.15)
His 238 NE2	O8	3.30 (0.03)
Asp 295 OD1	O8	2.63 (0.07)
Asp 296 OD2	N1	2.72 (0.06)
Zn^{2+}	O8	1.90 (0.04)

[a] Average for four independent molecules.

DCF or Pentostatin, a Natural Product Transition-State Analogue. The strong inhibitory effect of DCF on ADA activity has been attributed to the similarity of this natural product to the tetrahedral transition-state intermediate. The structure analysis reported here does show a DCF bound in a manner very similar to HDPR. This is particularly true for the coordination of the 8*R*-hydroxyl group of DCF to the Zn^{2+} which confers the strong potency and very high degree of stereoselectivity of inhibition by the analogue. Abrogation of this coordination is the main reason for the enormous decrease (about 7 orders of magnitude) in the inhibitory effect of the 8*S*-hydroxyl isomer relative to the 8*R* isomer (*7*). Moreover, the hydrogen-bonding interactions of His 238 and Asp 295 with the 8*R*-hydroxyl (Figure 4 and Table 4) will cease to exist with the 8*S*-hydroxyl. Replacement of the 8*R*-hydroxyl by an 8*S*-hydroxyl through modeling also places the 8*S*-hydroxyl group in an incompatible area surrounded by hydrophobic residues Leu 58, Phe 61, Thr 269, and Phe 300 (Figure 4B).

Substrate Conformation and Molecular Recognition. The two structures show excellent complementarity between the bound transition-state analogues and the active site (Figures 3 and 4). Very similar complementarity is also achieved in the binding of DAA, a ground-state analogue (*21*). This complementarity demonstrates the conformational requirements of bound substrates with respect to the following three well-established factors that contribute to the flexibility of purines/pyrimidines: (i) rotation about the glycosyl bond (C1′−N for purine) which is defined by the endocyclic torsion angle χ (O4′−C1′−N9−C4), (ii) rotation about the C4′−C5′ link represented by the excocyclic torsion angle γ (O5′−C5′−C4′−C3′), and (iii) ribose puckering. In the bound HDPR, DCF, and DAA, the position of the base relative to the sugar moiety is in the anti conformation with χ values confined to a narrow range (−106° to −111°). This finding is consistent with experimental evidence that adenosine can be deaminated by ADA only in its anti conformation (*22*, *48*). The orientation about the C4′−C5′ bond, for all three ligands, is +*sc* (gauche, gauche) with γ values from 54° to 57°. The three ligands are bound with a C3′ endo ribose pucker (e.g., see Figures 3 and 4).

Chemical features for substrate specificity of ADA, as first revealed in the structure of the complex with HDPR at pH 4.2 (*2*), are solidified by both pH 7 structures reported here. These include the requirements for the presence of ribose and the lone pairs in both N3 and N7.

An unusual aspect of substrate and inhibitor recognition, clarified by the pH 7 structures, is the hydrogen bond between the lone pair of N7 of HDPR or N1 of DCF and Asp 296 OD2 (Figures 3 and 4 and Tables 3 and 4). A similar hydrogen bond (2.7 Å distance) is also formed with

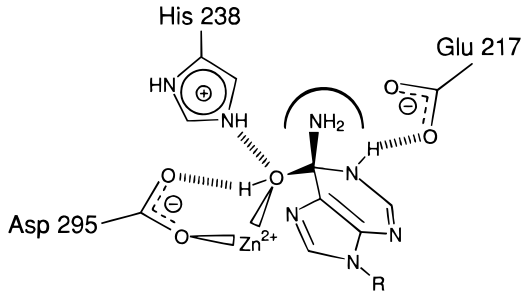

FIGURE 6: Schematic diagram of a tetrahedral transition-state intermediate of the ADA catalyzed reaction. The diagram is based on the structures of ADA with bound HDPR and the modeling the 6-NH_2. The 6-NH_2 would be close to an area bounded by Leu 58, Phe 61, Thr 269, and Phe 300.

N7 of the bound DAA (*21*). This interaction, also seen in the pH 4.2 structures, dictates that the side chain of Asp 296 has an abnormally high pK_a in order to serve as a hydrogen bond donor to the lone pair of the very basic nitrogen. The structures indicate two features in the environment of Asp 296 conducive to an elevated pK_a. The Asp residue is in the vicinity of hydrophobic residues Phe 61 and Phe 300 (Figures 3 an 4) and Phe 65 and Ile 299 (not shown). Additionally, a protonated (COOH) Asp 296 side chain is an outcome of being close to the COO^- of Asp 295, which is coordinated to the Zn^{2+}.

Catalytic Mechanism. In light of the pH 7 structures of the complexes with HDPR and DCF and recent site-directed mutagenesis experiments (*27*, *39*, *40*), we have further evaluated the catalytic mechanism of ADA. ADA-catalyzed reaction may be viewed in two stages: an initial stereospecific hydroxide addition to the C6 of the substrate to form the tetrahedral transition-state intermediate and a final ammonia elimination to form the inosine product. The important players revealed by the structures are the Zn^{2+}, Glu 217, His 238, and Asp 295 (Figures 3 and 4). Figure 6 shows a schematic diagram of a tetrahedral intermediate, generated by modeling the 6-NH_2 leaving group, to the structure of the bound HDPR.

The structural analyses, combined with mutagenesis studies, have shed more light on the addition reaction than the elimination reaction. Features of the addition reaction are summarized as follows. First, by acting as a powerful electrophile, Zn^{2+} remains the key player in activating the attacking water molecule (*2*, *21*). A Zn^{2+}-bound hydroxide molecule was, in fact, observed in the structure of the ADA complexed with DAA (*21*). Second, Glu 217 OE1 is in excellent alignment (i.e., Figure 3 and Tables 3 and 5) to donate a proton to N1 of a substrate, thereby reducing the N1 to C6 double bond character and making the C6 more susceptible to nucleophilic attack and to transformation from sp^2 to sp^3 in the tetrahedral transition-state adduct (*2*). Third, His 238 assists in the formation and stabilization of the attacking hydroxide from the Zn^{2+}-bound water molecule (*2*). It is within hydrogen-bonding and charge coupling distance to the Zn^{2+}-bound hydroxide (Table 5). This role is consistent with the mutagenesis experiment indicating that the primary function of this residue, in its protonated positively charged species, is the electrostatic stabilization of the attacking OH^- (*39*). Fourth, by forming a hydrogen bond with the Zn^{2+}-bound activated water or hydroxide (i.e., Figure 3 and Table 3), the carboxylate of Asp 295 assists in correctly orienting the hydroxide oxygen in line for the addition to the C6 (*21*). And fifth, the locations of the Zn^{2+} and Asp 295 on the B face or pro-S face of the adenosine ring dictate the stereochemistry of the hydroxide addition.

Table 5: Distances Relevant to Catalytic Mechanism

		distance		
pH	ligand	protein	prot/ligand/H_2O	distance (Å)
7.0	HDPR	Glu 217 OE1	HDPR N1	2.8
			HDPR O6	4.1
			HDPR N6[a]	4.1
			H_2O 2870	3.0
4.2	DAA		Zn^{2+}-bound H_2O	3.8
7.0	HDPR	Glu 217 OE2	HDPR N1	3.5
			HDPR O6	3.8
			HDPR N6[a]	3.3
			His 238 NE2	3.3
			H_2O 2280	2.4
4.2	DAA		Zn^{2+}-bound H_2O	3.8
7.0	HDPR	Asp 295 OD1	HDPR O6	2.8
			HDPR N6[a]	3.6
			His 238 NE2	3.6
			Asp 296 OD2	3.5
			Ser 265 OG	2.6
7.0	HDPR	His 238 NE2	HDPR O6	3.2
			HDPR N6[a]	4.7
4.2	DAA		Zn^{2+}-bound H_2O	2.8

[a] N6 was modeled with proper geometry and distance to C6 in the bound HDPR to simulate a tetrahedral transition-state intermediate.

The identity of the basic group that presumably abstracts a proton from the Zn^{2+}-bound water molecule in the addition reaction remains problematical. His 238, by possessing a pK_a in the pH range (5.5−8.5) of maximum activity for murine ADA (*26*) and by being within hydrogen-bonding distance to the Zn^{2+}-bound water molecule in the structure of ADA−DAA complex (Table 5), was proposed as the general base (*21*), but recent site-directed mutagenesis study of this residue provides little support for this proposal (*39*). Although the His mutant enzymes exhibited considerable loss of activity, one mutant with an Ala substitution was determined by X-ray and NMR spectroscopy to convert PR to HDPR.

We are left to consider Glu 217 as the general base. This consideration was guided by site-directed mutagenesis studies indicating that amino acid substitutions of Glu 217 resulted in enzyme mutants with very severe loss of activity (*27*, *49*) and with complete inability, as detected by NMR technique, to catalyze the conversion of PR to HDPR (*27*). Glu 217 OE1 is a logical choice for water proton abstraction since it, in turn, is in an excellent position (Tables 3 and 5) to donate a proton to N1. However, the distances (3.8 Å) of Glu 217 OE1 or OE2 to the Zn^{2+}-bound activated water or hydroxide in the structure of the ADA−DAA complex (Table 5) (*21*) are not ideal for abstraction of a water proton.

The ammonia elimination pathway is less understood. We consider two similar pathways, both with varying degrees of ambiguity. In one pathway, Glu 217 OE2 could, in the same manner proposed for a Glu residue in the CDA mechanism (*43*), shuttle the proton from 6-OH to the 6-NH_2 of the tetrahedral intermediate and, in the process, promote the elimination by way of a purinolate (6-O^-) intermediate (discussed further in the following section comparing the ADA and CDA). His 238 should further enhance the formation of the purinolate in much the same way as in the formation of the hydroxide in the water activation process.

A similar pathway could use Asp 295 OD1 as the conduit of the proton from 6-OH to the 6-NH_2. This role is primarily dictated by the close interaction of the OD1 with the hydroxyl group of HDPR or DCF (Figures 3 and 4 and Tables 3, 4, and 5); no other functional residues are as close to either OH group. However, the location of the OD1 (on the pro-S face of a transition state, Figures 3 and 6) and its long distance (3.6 Å, Table 5) relative to N6 on the pro-R side may not be ideal for proton transfer. Moreover, the coordination of the Asp OD2 with Zn^{2+} and the hydrogen bond between OD1 and Ser 265 OG may restrict the movement of Asp 295.

Whereas the 6-OH adduct of the transition-state intermediate is interacting with the Zn^{2+} and polar residues His 238 and Asp 295 (Figure 6), the modeled 6-NH_2 leaving group would be located in a hydrophobic area largely bounded by residues Leu 58, Phe 61, Thr 269, and Phe 300 (Figures 4B and 6). This incompatible location would further facilitate the elimination of the leaving group and to an essentially irreversible enzyme catalyzed chemical reaction.

Comparison between Adenosine Deaminase and Cytidine Deaminase. The structure of ADA is completely different from that of CDA (*2, 43*). ADA is a monomer whereas CDA is a homodimer. Considerable differences also exist between the active sites in the two enzymes. Zn^{2+} coordination in ADA, with bound potent inhibitors, is accomplished by five ligands (3 His, 1 Asp, and a hydroxyl group of the inhibitors or a water molecule) in a trigonal bipyramidal geometry, whereas that in CDA is achieved by four ligands (2 Cys, 1 His, and a hydroxyl group of transition-state analogues or a water molecule) in a nearly tetrahedral geometry. One of the coordinating Cys residues (Cys 132) in CDA, which is believed to have a unique role as a "valence buffer" that accommodates changing negative charge on the hydroxyl group (*50*), is not present in ADA. The catalytically important His 238 and Asp 295 residues of ADA are missing in CDA. Significantly more acidic residues are found in the active site of ADA than in CDA.

Glu 217 of ADA is equivalent to Glu 104 of CDA; however, they are in very different environments. Glu 217 is surrounded by bound ligand and Leu 58, Glu 186, Val 218, His 238, Thr 269, and Ala 271 (Figure 5). Moreover, whereas hydrogen bond networks, by way of water molecules, are associated with the ADA Glu side-chain oxygens in an anti orientation (Figure 5), none are apparently involved with the CDA Glu side chain. The functional significance of the environment and interaction of the ADA Glu residue is unclear. This environment is also very much different from those of similar catalytic residues in other zinc metalloenzymes.

Because ADA and CDA contain Zn^{2+}, along with the Glu residue in the favorable syn orientation, the most common features in the proposed catalytic mechanisms of both deaminases pertain to the hydroxide addition with the Zn^{2+} acting as a strong electrophile in the water activation and the Glu residue (OE1 moiety in both enzymes) donating a proton to N1 of adenosine or N3 of cytidine. These features are amply supported by crystallographic studies of both enzymes with bound inhibitors (*2, 21, 43, 44*).

The Glu residue is also assumed to be the general base for water activation in both ADA and CDA, a role which has precedence in enzymes with Zn^{2+} cofactor (*41*). However, the distances of the Glu carboxylate group (OE1) to the Zn^{2+}-bound water molecule are somewhat long, 3.8 Å in the ADA structure complexed with DAA (*21*) and 3.7 and 3.3 Å in the structures of CDA complexed with 3,4-dihydrozebularine (*44*) and 3-deazacytidine (*50*), respectively.

Because Glu 104 OE2 of CDA makes a short hydrogen bond with the 4-OH of bound transition-state analogues, it has been proposed as the proton shuttle in the elimination reaction pathway, abstracting the proton from the 4-OH of the tetrahedral transition-state intermediate and transferring it to the leaving 4-NH_2 in the course of the tautomerization reaction of the tetrahedral intermediate by way of a pyrimidinolate (4-O^-) (*43, 44*). The homology of this pathway in ADA employs Glu 217 OE2 or Asp 295 OD1 as a conduit of the proton (see above).

With the exception of the interaction between Glu 217 OE1 and N1 of HDPR or N6 of DCF (Tables 3 and 4), which is relevant to both addition and elimination reactions (see above), the Glu 217 carboxylate side chain makes no other favorable interactions with bound analogues (Table 5). For this reason, Glu 217 OE2 is not as ideal a vehicle for a proton transfer from 6-OH to 6-NH_2 as Glu 104 OE2 of CDA. Moreover, Glu 217 OE2 has to abstract, at a long distance, the proton of the 6-OH, which is hydrogen bonded to Asp 295 OD1 (Table 5), a feature not present in CDA.

Although Glu 217 OE2 is far from 6-OH of HDPR and the modeled 6-NH_2 (Table 5), it is juxtaposed between these two moieties of a transition state (with reference to Figure 3). Thus, the geometry of OE2, as a possible proton shuttle, is somewhat more favorable than that of Asp 295 OD1 (see above).

For Glu 217 to play a role in proton transfer in the elimination reaction, as well as a general base in the addition reaction, requires considerable flexibility in its side chain, a feature completely lacking evidence from structural data obtained thus far. In all the structures (∼a dozen) of native and mutant enzymes with bound ligands (HDPR, DCF, DAA, and inosine), at pH 4.2 and 7.0 and in three different crystal lattice systems, Glu 217 is seen in identical position with its side chain in a fully extended conformation (e.g., Figures 3, 4, and 5). This position is very much restricted by being close to bound ligands and several residues (Figure 5). The entire side chain of Glu 217 is hemmed in on one side by Leu 58 and Val 218 and on the other side by His 238. Furthermore, the carboxylate of Glu 217 is held in place by water-mediated networks of hydrogen bonds with other residues (Figure 5). Flexibility of Glu 217 may additionally require movement of the hairpin loop (residues 214−221) deploying this residue. However, as the backbone and side chains of the loop are engaged in numerous interactions with residues from two other flanking loops (residues 237−242 and 182−186), this movement is unlikely and has not been observed in any of the dozen structures.

Conclusion. Our crystallographic studies have shown that the mode of binding of HDPR to ADA at pH 7, where the enzyme is fully active, is essentially identical for four independent molecules. Moreover, this binding mode is indistinguishable from that previously observed in the ADA−HDPR structure at pH 4.2 where the enzyme is 20% active. These studies further demonstrate very similar binding of DCF. The strong inhibition by DCF and HDPR (K_i in the

picomolar range) is attributed mainly to the stereospecific coordination of the hydroxyl group of the inhibitors to the Zn^{2+} cofactor. The hydroxide addition process of the catalytic mechanism is very similar to that of CDA. Owing to some dissimilarities of the active sites between ADA and CDA, the ammonia elimination reaction pathways may be different between the two enzymes. The ability to crystallize ADA at pH 7 and in four independent molecules, along with its many advantages, will enable us to extend our crystallographic studies to binding of other ligands and, thereby, obtain a fuller understanding of enzyme function.

ACKNOWLEDGMENT

We thank Dr. David K. Wilson for technical advice and helpful discussions and William E. Meador for technical assistance. We are grateful to Dr. Frederick M. Rudolph for continued interest. Further helpful discussion with Dr. Vera Sideraki is gratefully acknowledged.

REFERENCES

1. Schmidt, Z. (1932) *Z. Physiol. Chem. 208,* 185−224.
2. Wilson, D. K., Rudolph, F. B., and Quiocho, F. A. (1991) *Science 252,* 1278−1284.
3. Sawa, T., Fukagawa, Y., Homma, I., Takeuchi, T., and Umezawa, H. (1967) *J. Antibiot. 20,* 227−231.
4. Woo, P. W. K., Dion, H. W., Lange, S. M., Dahl, L. F., and Durham, L. J. (1974) *J. Heterocycl. Chem. 11,* 641−643.
5. Agarwal, R. P., Spector, T., and Parks, R. E., Jr. (1977) *Biochem. Pharm. 26,* 359−367.
6. Agarwal, R. P., Cha, S., Crabtree, G. W., and Parks, R. E., Jr. (1978) in *Chemistry and Biology of Nucleosides and Nucleotides* (Harmon, R. E., Robins, R. K., and Townsend, L. B., Eds.) pp 159−197, Academic Press, New York.
7. Schramm, V. L., and Baker, D. C. (1985) *Biochemistry 24,* 641−6.
8. Spiers, A. S. D., Moore, D., Cassileth, P. A., Harrington, D. P., Cummings, F. J., Neiman, R. S., Bennett, M. J., and O'Connell, M. J. (1987) *N. Engl. J. Med. 316,* 825−830.
9. Cummings, F. J., Crabtree, G. W., Wiemann, M. C., Spremulli, E. N., Parks, R. E., Jr., and Calabresi, P. (1988) *Clin. Pharmacol. Therapeut. 44,* 501−509.
10. Kredich, N. M., and Hershfield, M. S. (1989) in *The metabolic basis of inherited disease* (Scriver, C. R., et al., Eds.) pp 1045−1075, McGraw-Hill, New York.
11. Lee, P. C. (1973) *Dev. Biol. 31,* 227−233.
12. Chinsky, J. M., Ramamurthy, V., Fanslow, W. C., Ingolia, D. E., Blackburn, M. R., Shaffer, K. T., Higley, H. R., Trentin, J. J., Rudolph, F. B., and Knudsen, T. B. (1990) *Differentiation 42,* 172−183.
13. Hong, L., Mulholland, J., Chinsky, J. M., and Knudsen, T. B. (1991) *Biol. Reprod. 44,* 83−93.
14. Kurz, L. C., Moix, L., Riley, M. C., and Frieden, C. (1992) *Biochemistry 31,* 39−48.
15. Wolfenden, R., Kaufman, J., and Macon, J. B. (1969) *Biochemistry 8,* 2412−2415.
16. Evans, B. E., and Wolfenden, R. V. (1973) *Biochemistry 12,* 392−398.
17. Kurz, L. C., and Frieden, C. (1983) *Biochemistry 22,* 382−389.
18. Yang, C., Carlow, D., Wolfenden, R., and Short, S. A. (1992) *Biochemistry 31,* 4168−4174.
19. Moore, J. T., Silversmith, R. E., Maley, G. F., and Maley, F. (1993) *J. Biol. Chem. 268,* 2288−2291.
20. Merkler, D. J., and Schramm, V. L. (1993) *Biochemistry 32,* 5792−5799.
21. Wilson, D. K., and Quiocho, F. A. (1993) *Biochemistry 32,* 1689−1694.
22. Ikehara, M., and Fukui, T. (1974) *Biochim. Biophys. Acta 338,* 512−519.
23. Jones, W., Kurz, L. C., and Wolfenden, R. (1989) *Biochemistry 28,* 1242−1247.
24. Kati, W. M., and Wolfenden, R. (1989) *Science 243,* 1591−1593.
25. Wilson, D. K., and Quiocho, F. A. (1994) *Nat. Struct. Biol. 1,* 691−694.
26. Sharff, A. J., Wilson, D. K., Chang, Z., and Quiocho, F. A. (1992) *J. Mol. Biol. 226,* 917−921.
27. Mohamedali, K. A., Kurz, L. C., and Rudolph, F. B. (1996) *Biochemistry 35,* 1672−1680.
28. Wilson, D. K., Rudolph, F. B., Harrison, M. L., Kellems, R. E., and Quiocho, F. A. (1988) *J. Mol. Biol. 200,* 613−614.
29. Otwinowski, Z., and Minor, W. (1997) *Methods Enzymol. 276,* 307−326.
30. Brünger, A. T. (1992) *X-PLOR, Version 3.1, A system for X-ray crystallography and NMR,* Yale University, New Haven, CT.
31. Engh, R. A., and Huber, R. (1991) *Acta Crystallogr., Sect. A 47,* 392−400.
32. Sack, J. S., and Quiocho, F. A. (1997) *Methods Enzymol. 277,* 158−173.
33. Brünger, A. T. (1992) *Nature 355,* 472−474.
34. Kleywegt, G. J., and Brünger, A. T. (1996) *Structure 4,* 897−904.
35. Jiang, J. S., and Brünger, A. T. (1994) *J. Mol. Biol. 243,* 100−115.
36. Weis, W. I., Brünger, A. T., Skehel, J. J., and Wiley, D. C. (1990) *J. Mol. Biol. 212,* 737−761.
37. Braig, K., Adams, P. D., and Brünger, A. T. (1995) *Nat. Struct. Biol. 2,* 1083−1094.
38. Cox, M. B., Arjunan, P., and Arora, S. K. (1990) *J. Biomol. Struct. Dyn. 8,* 199−212.
39. Sideraki, V., Wilson, D. K., Kurz, L. C., Quiocho, F. A., and Rudolph, F. B. (1996) *Biochemistry 35,* 15019−15028.
40. Sideraki, V., Mohamedali, K. A., Wilson, D. K., Chang, Z., Kellems, R. E., Quiocho, F. A., and Rudolph, F. B. (1996) *Biochemistry 35,* 7862−7782.
41. Lipscomb, W. N., and Sträter, N. (1997) *Chem. Rev. 96,* 2375−2433.
42. Tainer, J. A., Getzoff, E. D., Beem, K. M., Richardson, J. S., and Richardson, D. C. (1982) *J. Mol. Biol. 160,* 181−217.
43. Betts, L., Xiang, S., Short, S. A., Wolfenden, R., and Carter, C. W., Jr. (1994) *J. Mol. Biol. 235,* 635−656.
44. Xiang, S., Short, S. A., Wolfenden, R., and Carter, C. W., Jr. (1995) *Biochemistry 34,* 4516−4523.
45. Tronrud, D. E., Ten Eyck, L. F., and Matthews, B. W. (1987) *Acta Crystallogr., Sect. A 43,* 489−501.
46. Gandour, R. D. (1981) *Bioorg. Chem. 10,* 169−176.
47. Gandour, R. D., Nabulsi, N. A. R., and Fronczek, F. R. (1990) *J. Am. Chem. Soc. 112,* 7816−7817.
48. Zemlicka, J. (1975) *J. Am. Chem. Soc. 97,* 5896−5903.
49. Bhaumik, D., Medin, J., Gathy, K., and Coleman, M. S. (1993) *J. Biol. Chem. 268,* 5464−5470.
50. Xiang, S., Short, S. A., Wolfenden, R., and Carter, C. W., Jr. (1996) *Biochemistry 35,* 1335−1341.
51. Ferrin, T. E., Huang, C. C., Jarvis, L. E., and Langridge, R. (1988) *J. Mol. Graph. 6,* 13−27.

BI980324O